Research Article Vol. 2, No. 2 / February 2015 / Optica 88

Micrometer-scale integrated silicon source of time-energy entangled photons

DAVIDE GRASSANI,[1] STEFANO AZZINI,[1] MARCO LISCIDINI,[1] MATTEO GALLI,[1] MICHAEL J. STRAIN,[2,3] MARC SOREL,[2] J. E. SIPE,[4] AND DANIELE BAJONI[5,*]

[1]Dipartimento di Fisica, Università degli Studi di Pavia, via Bassi 6, 27100 Pavia, Italy

[2]School of Engineering, University of Glasgow, Glasgow G12 8LT, UK

[3]Institute of Photonics, University of Strathclyde, Glasgow G4 0NW, UK

[4]Department of Physics and Institute for Optical Sciences, University of Toronto, 60 St. George Street, Ontario, Canada

[5]Dipartimento di Ingegneria Industriale e dell'Informazione, Università degli Studi di Pavia, via Ferrata 1, Pavia, Italy

*Corresponding author: daniele.bajoni@unipv.it

Received 17 September 2014; revised 18 November 2014; accepted 20 November 2014 (Doc. ID 223278); published 26 January 2015

Entanglement is a fundamental resource in quantum information processing. Several studies have explored the integration of sources of entangled states on a silicon chip, but the devices demonstrated so far require millimeter lengths and pump powers of the order of hundreds of milliwatts to produce an appreciable photon flux, hindering their scalability and dense integration. Microring resonators have been shown to be efficient sources of photon pairs, but entangled state emission has never been proven in these devices. Here we report the first demonstration, to the best of our knowledge, of a microring resonator capable of emitting time-energy entangled photons. We use a Franson experiment to show a violation of Bell's inequality by more than seven standard deviations with an internal pair generation exceeding 10^7 Hz. The source is integrated on a silicon chip, operates at milliwatt and submilliwatt pump power, emits in the telecom band, and outputs into a photonic waveguide. These are all essential features of an entangled state emitter for a quantum photonic network.

OCIS codes: (270.0270) Quantum optics; (250.5300) Photonic integrated circuits; (270.5565) Quantum communications; (230.5750) Resonators; (120.3180) Interferometry.

http://dx.doi.org/10.1364/OPTICA.2.000088

1. INTRODUCTION

Photonics is increasingly seen as an attractive platform for quantum information processing [1–4]. In quantum cryptography [2,5] photons have several advantages as vectors of information, due to their long coherence times at room temperature and the possibility of being transmitted over the existing optical fiber infrastructure. The potential scalability and integrability of photonics also suggests its application in quantum simulation and computing [6–9]. The most common strategy for producing entangled photon pairs at room temperature is the use of the parametric fluorescence that can occur in a nonlinear crystal [10–12]. While having high generation rates, these sources are very difficult to integrate. An ideal integrated source of entangled photons should be CMOS compatible for cost-effective and reliable production, easily interfaced with fiber networks for long-range transmission in the telecom band, and take up little "real estate" on the chip. For such sources the main results have been obtained by exploiting third-order nonlinearities in silicon, in studies that have been focused on the generation of qubits based on polarization entangled photon pairs [13,14] or entangled time-bins [15,16] in long waveguiding structures. However, these devices require lengths ranging from fractions of a millimeter to centimeters to produce an appreciable photon pair flux, hindering their scalability.

Another kind of quantum correlation of photon pairs is *time-energy* entanglement. This is arguably the most suitable

format for the entanglement of photons, as it can be easily manipulated in integrated optical circuits [8], and it can be preserved over long distances in the fiber optical networks [17,18] needed for communication between devices. Very recently, it has been shown that the use of time-energy entangled photon pairs in quantum key distribution can enable a higher key generation rate compared to entangled photon pairs in lower-dimensional Hilbert spaces [19].

In this work we demonstrate that silicon ring resonators in a silicon-on-insulator platform are an efficient source of time-energy entangled photon pairs. Large field enhancements can be obtained in resonant structures [20,21], and ring resonators in particular [22,23]. Combined with the large effective nonlinearities achievable in silicon ridge waveguides, of which they are made, this allows the reduction of the emitter's footprint by orders of magnitude over other sources. There is then a drastic improvement of the wavelength conversion efficiency, together with the spectral properties of the emitted pairs, with respect to silicon waveguide sources.

2. SAMPLE STRUCTURE AND TRANSMISSION SPECTRA

The sample geometry is illustrated in Fig. 1(a): the device is a ring resonator with a radius of 10 μm, evanescently coupled to a straight silicon waveguide on one side of the ring; both the ring and the waveguide have transverse dimensions of 500 nm (width) and 220 nm (height) and are etched on a silicon-on-insulator wafer. The gap between the ring and the waveguide is 150 nm. The coupling of light onto and off the chip is implemented by mode field converters, and the emission is extracted through a tapered optical fiber. A tunable continuous wave laser is used for characterizing the sample, and as a pump for the nonlinear optical experiments (see Supplement 1). While such ring resonators would act as all-pass devices in the absence of scattering losses, they are somewhat akin to integrated Fabry–Perot cavities in that the modes of the electromagnetic field are identified by a comb of resonances. The transmission spectrum from our sample is shown in Fig. 1(b), where the dips occur due to scattering losses at the resonances. The free spectral range is about 9 nm, and the resonance quality factors (Qs) are, on average, around 15,000. The minimum transmission is about 3%–5% on resonance, meaning that the ring almost satisfies the critical coupling condition, which maximizes the coupling between the ring and the bus waveguide.

3. NONLINEAR SPECTROSCOPY AND COINCIDENCE MEASUREMENTS

The nonlinear process responsible for the generation of photon pairs is spontaneous four-wave mixing (SFWM) [23–27]: two pump photons at frequency ω_p are converted into signal and idler photons at frequencies ω_s and ω_i [as sketched in the inset of Fig. 1(b)]. When using resonant structures, energy conservation implies three equally spaced resonances in energy ($\hbar\omega_s + \hbar\omega_i = 2\hbar\omega_p$). Another advantage in using ring resonators is that the process is greatly amplified by the resonance, and it has been shown [28] that the generation rate goes as

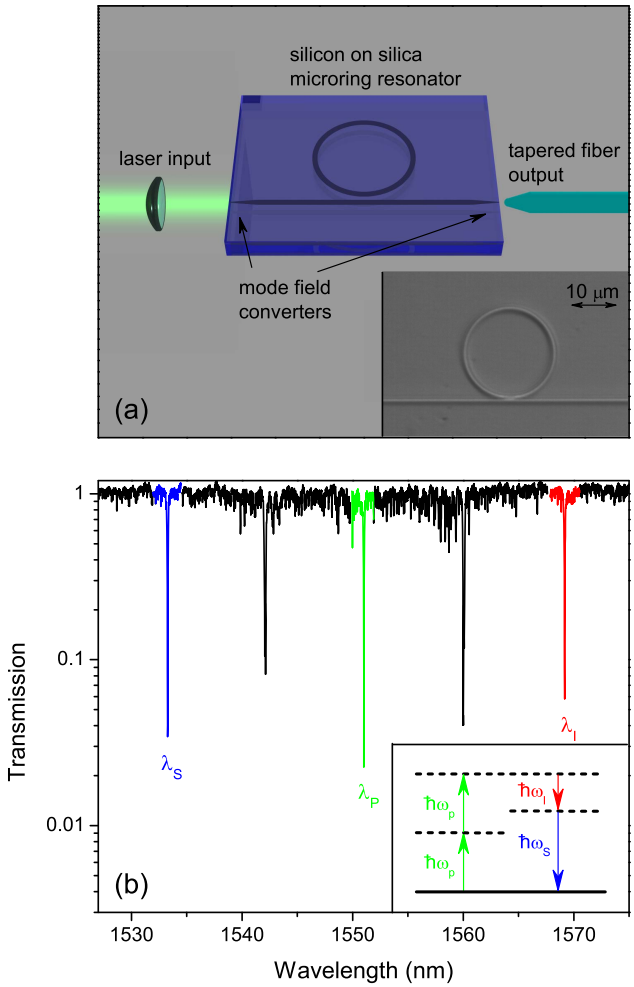

Fig. 1. Sample structure and characterization. (a) Sketch of the sample together with the input/output light coupling mechanism. The R = 10 μm ring resonator is evanescently coupled to a silicon nanowire waveguide via a deep-etched 150 nm gap point coupler. An optical microscope image of the ring is shown in the inset. The waveguide ends at both sides with spot-size converters: 300 μm long silicon inverse tapers ending in a 20 nm tip width covered by 1.5 μm × 2.0 μm polymer waveguides. Light injection from a collimated pump laser is achieved by the use of an aspheric lens with numerical aperture NA = 0.5. The output from the sample is collected with a PM lensed fiber with a working distance of 3 μm. (b) Transmission spectrum of the resonator. The pump resonance is highlighted in green, and the signal and idler resonances employed in the experiment are indicated in blue and red, respectively.

$R \propto Q^3 P^2 r^{-2}$, where Q is the quality factor of the resonances, r is the ring's radius, and P is the pump power. In our ring resonators, waveguide dispersion limits the bandwidth over which pairs can be generated for a fixed pump wavelength to a spectral range of about 80 nm, resulting in a plentiful choice of possible signal and idler pairs. We have also verified that the generation rate is almost the same for all resonances up to the fourth neighboring resonances from the pump [28]. Thus the pump can generate a number of entangled signal and idler pairs in parallel, with each entangled pair easily separated from the others because of their frequencies. In this work we study only one pair, as highlighted by colors in Fig 1(b): we use a resonance around 1550 nm (at the center

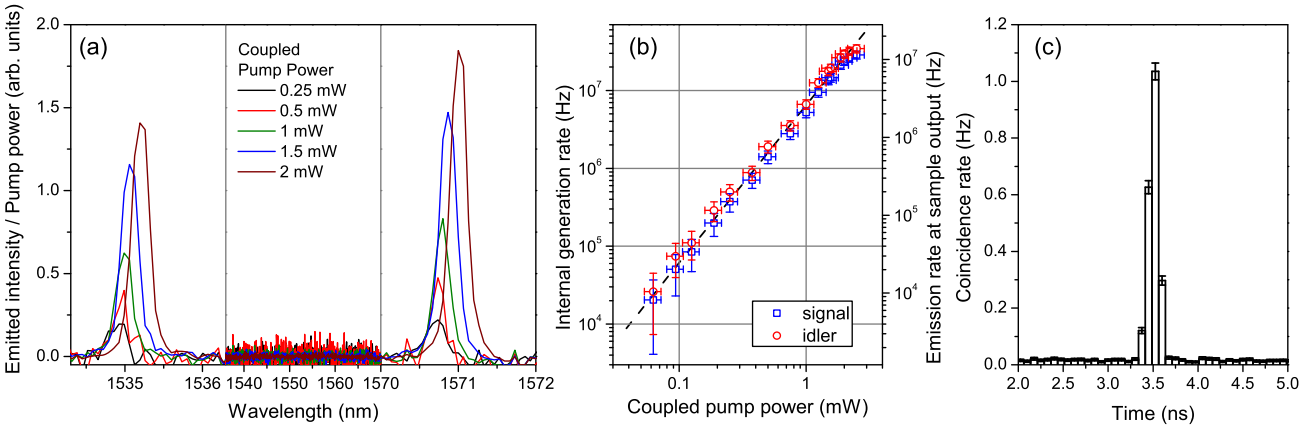

Fig. 2. SFWM and coincidences. (a) Spectra of the SFWM experiment for five different coupled pump powers; signal and idler intensities are divided by the corresponding pump power to underline the superlinear growth of the intensity. The slight difference in intensity between the two peaks is due to slightly different coupling to the input/output bus of the signal and idler modes. For coupled pump powers above 1 mW, the pump wavelength was retuned to compensate the red shift of the resonance due to the thermo-optic effect [22]. The horizontal scale is expanded around the signal and idler resonances, while the complete absence of detected photons at the pump resonance confirms the excellent rejection of the transmitted pump intensity in the setup. (b) Scaling of the internal generation rates of signal (blue squares) and idler (red circles) photons in SFWM, varying the coupled pump power. The black dashed line is a guide to the eye proportional to the square of the pump power. The left axis indicates the photon flux measured at the sample output. (c) Measured coincidence histogram for a coupled pump power $P_p = 1$ mW. The time resolution is 75 ps, and it is driven by the response time of the detectors.

of the telecommunication c-band) for the pump and its second nearest neighbor resonances for the signal and idler; this spectral distance is chosen to optimize filtering of the laser background noise at the signal and idler frequencies.

FWM spectra are shown in Fig. 2(a): two clear peaks of generated photons are evident at the signal and idler frequencies. It is important to notice that the pump laser is completely filtered out, so that only spontaneously generated photons are detected. The parametric nature of the emission process is confirmed by the superlinear increase of the generation rate with increasing pumping powers: the quadratic behavior of the generated beams is reported in Fig. 2(b), where we plot the estimated generation rate of photon pairs inside the ring resonator together with the output rate [28]. The output rate was directly measured at the sample output, as detailed in Supplement 1. The internal generation rate was estimated in the following way: we have directly measured a total insertion loss of 7 dB for the sample. Due to the sample symmetry, we assume propagation and coupling losses from the ring resonator to the output fiber to be 3.5 dB. The internal generation rate is then estimated from the flux measured at the output by subtracting the 3.5 dB.

The generation rate can exceed 10^7 Hz; this is an extremely high rate, and will be beneficial for all experiments involving coincidence counting. The first step necessary to verify entanglement is to check that signal and idler photons are emitted in pairs: this was assessed via a coincidence experiment, in which the relative times of arrival of idler and signal photons were statistically analyzed [26]. The coincidence measurement shown in Fig. 2(c) is obtained employing the setup described in Fig. 3(a) (detailed in Figure S1 of Supplement 1) by masking the short arm of each interferometer. The total losses undergone by the signal and idler in the coincidence experiment are 31 and 34 dB, respectively.

An instance of a histogram of the arrival times is shown in Fig. 2(c), where a distinct coincidence peak is visible over a small background of accidental counts; this is a clear signature of the concurrent emission of the signal–idler pairs. The 3.5 ns offset is determined by the different path lengths of the signal and idler photons. The coincidence measurements, for experimental consistency, were taken using the same setup used to measure the entanglement as described below, by masking one arm in each interferometer. The losses from the setup were directly measured for each component, and amount to 31 dB for signal photons and 34 dB for idler photons, giving a total loss of 64 dB on the coincidence rate. Almost all of these losses, as discussed in Supplement 1, are outside the source and are mainly given by the interferometers and the low quantum efficiency of the detectors used in these experiments.

Accidental counts are primarily due to emitted pairs of which only one photon is detected. The accidentals in the coincidence curve mainly come from the detection of signal and idler photons belonging to different pairs. As all emission times are equivalent, the signal-to-noise ratio (SNR) is also an indication of how likely it is for multiple pairs to be generated at the same time [29]. In our case the SNR is about 65 in Fig. 2(c), and higher than 100 in some of the measurements (see Supplement 1).

4. ENTANGLEMENT TEST ON THE EMITTED PHOTON PAIRS

The photon pairs are emitted simultaneously, but, because of the continuous wave pumping, the emission time is indeterminate to within the coherence time of the pump laser; this is several microseconds in our experiments. This systematic lack of information can lead to the pairs being time-energy entangled, as first pointed out by Franson [30]. In order to

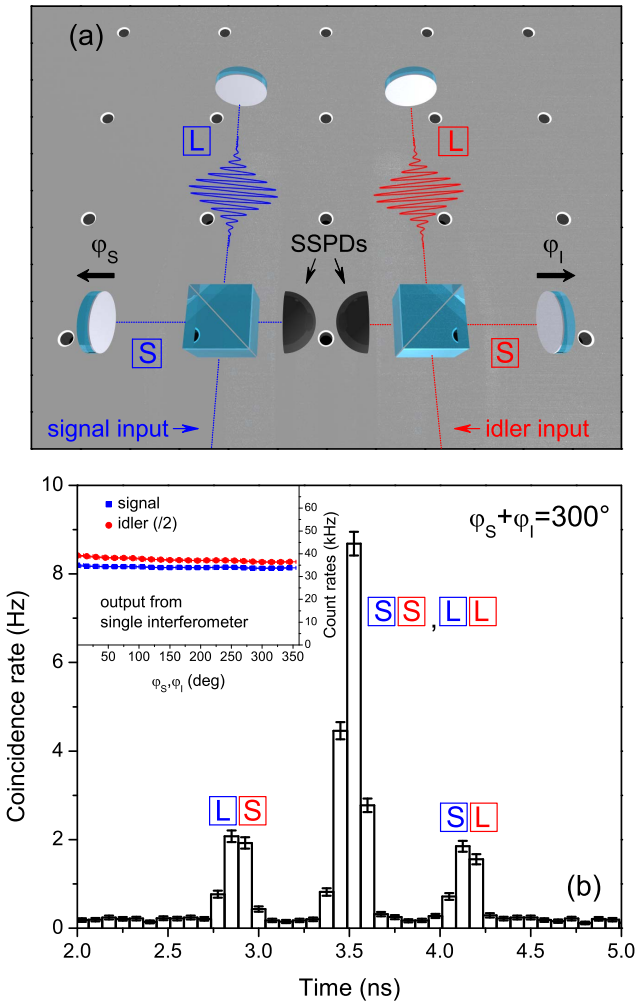

Fig. 3. Correlations at the output of a double interferomenter. (a) Sketch of the signal and idler Michelson interferometers. The arm length difference of the two interferometers is the same to well within the coherence length of the generated photons (Supplement 1). The movable mirrors on the short arms are connected to a piezo actuator and are used to control the relative phase between the short and long arms. At the outputs of the interferometers are two superconducting single-photon detectors (SSPDs). (b) Instance of coincidence histogram measured at the output of the interferometers, taken for a coupled pump power of 1.5 mW. The integration time is 120 s. The error bars indicate the error on the counts. The inset shows the absolute intensity at the output of each interferometer while varying the respective phase: the complete absence of interference confirms that the arm length difference is much larger than the coherence time on the generated photons.

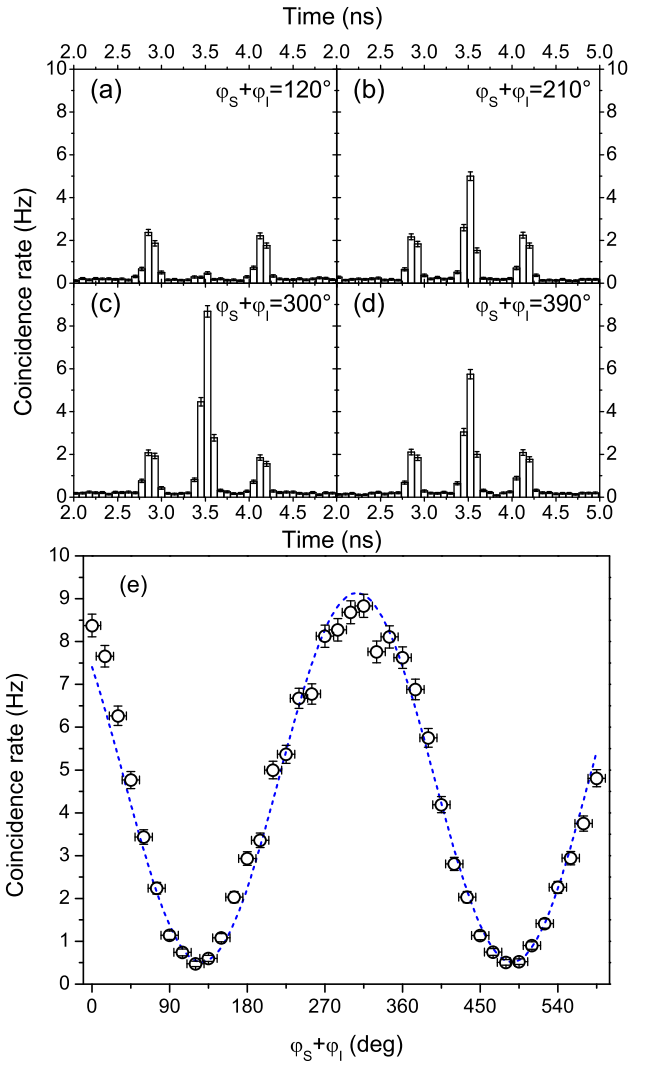

Fig. 4. Entanglement between signal and idler photons. (a)–(d) Histograms of the coincidence rate for four different phase settings. (e) Two-photon interference of the double interferometer configuration: the coincidence count rate of the central peak is plotted as a function of the phase $\varphi_s + \varphi_i$. The integration time is 120 s for each point, and the pump power is 1.5 mW. The dotted black curve is a best fit of the experimental data.

experimentally measure the entanglement we have used a double interferometer [30,31], as shown in Fig. 3(a). Photons at idler frequencies enter one interferometer, while photons at signal frequencies enter the other [Fig. 3(a)]. The unbalanced ΔT between the two arms of the interferometers must be much greater than the coherence time τ of the signal and idler photons to avoid first-order interference. In our case $\Delta T \sim 0.67$ ns while $\tau \sim 10$ ps (τ was extracted from the linewidth of the modes).

The absence of interference in each single interferometer was verified by varying the path differences independently in each of the interferometers and confirming that there was no change in the counting rate detected by the superconducting single-photon detectors (SSPDs), as shown in the inset of Fig. 3(b). Then with the interferometer arms fixed [32] we measured the arrival time of idler photons with respect to signal photons [Fig. 3(b)]; the generated histograms reveal three relative arrival times. The earliest peak is due to the signal photon having taken the long path in the interferometer and the idler photon having taken the short path; the reverse holds for the latest peak. The middle peak is due to two indistinguishable paths, both photons taking the long path or both taking the short path. The inability to distinguish from which of these two cases the coincidence event arises, due to the long coherence time of the pump, causes second-order interference [30]. The coincidence rate for the central peak is expected to be

$$C(\varphi) = 2C_0(1 + \cos(\varphi + \vartheta)), \quad (1)$$

where C_0 is the detected coincidence rate measured by covering one arm in each interferometer. Since signal and idler photons propagate in the same direction once they exit the sample, the phase term φ in the above expression is given by the sum of the phases acquired by the photons passing through the long arms with respect to the short ones, $\varphi = \varphi_S + \varphi_I$, and ϑ is a constant phase term dependent on the unknown actual lengths of the interferometer arms.

The effect of varying φ is shown in Fig. 4; the full experimental dataset is shown in Figs. S4 and S5 of Supplement 1. While the side peaks, corresponding to distinguishable events, have heights that are independent of φ, the number of coincidence counts of the central peak oscillates between minima, close to zero events, and a maximum, close to four times the height of the side peaks, as shown in Figs. 4(a)–4(d). The height of the central peak as a function of φ is summarized in Fig. 4(e). The trend is well fitted by a sinusoid curve of the type of Eq (1). For the raw data of Fig. 4(e), the best fit yields a visibility $V_{\text{Meas}} = 89.3\% \pm 2.6\%$ (greather than $1/\sqrt{2}$), proving a violation of Bell's inequality by 7.1 standard deviations, and so we can conclude that we are generating time-energy entangled photon pairs [33].

5. DISCUSSION

The experiment was performed for various pumping powers P (see Fig. S6 of Supplement 1 for the data), and the results are summarized in Table 1. Bell's inequality is violated in all cases, and by more that 11 standard deviations in the best case. The visibility is limited by the background due to emission of multiple couples and possibly other parasitic luminescent processes, such as FWM and Raman scattering in the access waveguide and in the optical fibers in the setup. The SNR, as expected, decreases with increasing pumping power, but it is always sufficiently high to lead to entanglement. It is worth noticing that the values of the measured visibility V_{Meas} reported in the table are obtained by a single fit operation on the raw data without performing any data correction, e.g., without subtracting the dark counts of the detectors. Finally, the maximum measurable visibility is limited by the first-order visibility of the interferometers, in our setup $w = 0.95$, which gives the expected visibility $V = V_{\text{Meas}}/\text{w}$ (see the last column of Table 1).

In conclusion, we have experimentally demonstrated a microstructured, CMOS-compatible source of entangled photons, operating at room temperature with unprecedented capabilities. While ring resonators have long been studied theoretically as a source of quantum correlated states, and pairs of photons emitted from spontaneous FWM in silicon ring resonators have been detected, with this work the oft-quoted promise that these devices could serve as sources of entangled photons has finally been fulfilled. We confirmed the violation of Bell's inequality by more than seven standard deviations, and we demonstrated the generation of time-energy entangled photon pairs particularly relevant for telecommunication applications. The source has incomparable operating characteristics. Beyond the high purity of the emitted two-photon states, the spectral brightness per coupled pump power is remarkable, at about 6×10^7 nm^{-1} mW^{-2} s^{-1}. This is more than four order of magnitudes larger than that reported for entangled photon pairs emitted by long silicon waveguides [13,15,23]. Even when compared to room temperature sources of entangled photons based on χ^2 nonlinearities, which are typically not CMOS compatible, the emission rate reported here is remarkable. It is two orders of magnitude larger than that obtained from GaAs-based waveguides [34] for 1 mW of coupled pumping power and, for the given bandwidth, is of the same order of magnitude as the emission rate of *centimeter* long waveguides in periodically poled crystals [11] (see Table 2), while having a footprint of a few hundred square micrometers. This small footprint has great advantages for scalability: all the existing know-how of integrated photonics can be directly applied with our source, and its micrometric size makes it ideal for integration with other devices on the same chip, such as integrated filters for the pump and the routing of signal and idler, for what integration strategies are well established. In particular, with quantum cryptography protocols in mind, one perspective for this work would be to take advantage of the silicon photonics industrial know-how to integrate the pump filtering and signal/idler demultiplexing stages on a single "transmitter" chip [35] and implement two "receiver" chips with integrated interferometers. Considering the receiving chips, the coherence time of the signal and idler photons in this work corresponds to a coherence length of about 1 mm in a silicon waveguide, and thus an arm unbalance of some centimeters would be needed in the interferometers; this can be easily achieved on chip using spiraled waveguides. The main problem hindering this goal is, for the moment, the unavailability of single-photon counters for the telecom band working at room temperature and integrated on a silicon chip.

Table 1. Violation of Bell Inequalities[a]

P (mW)	R (MHz)	SNR	V_{Meas} (%)	$\frac{V_{\text{Meas}}-1/\sqrt{2}}{\sigma_{V_{\text{Meas}}}}$	V (%)
0.25 ± 0.025	0.4 ± 0.11	131.6 ± 16.5	94.8 ± 3.8	6.4	99.8 ± 4
0.5 ± 0.05	1.7 ± 0.3	120.4 ± 7.9	88.2 ± 4.8	3.6	92.8 ± 5.1
1.0 ± 0.1	5.8 ± 0.8	64.4 ± 3.3	91.8 ± 1.9	11.2	96.6 ± 2.0
1.5 ± 0.15	14 ± 1.9	45.1 ± 2.2	89.3 ± 2.6	7.1	94.0 ± 2.7
2.0 ± 0.2	27 ± 3.1	22.9 ± 1.0	83.8 ± 3.2	4.1	88.2 ± 3.4

[a]Summary of the measured parameters for five values of the coupled pump power P. R, pair emission rate; SNR, signal-to-noise ratio; V_{Meas}, visibility of the two-photon interference extracted from the experimental raw data; $(V_{\text{Meas}} - 1/\sqrt{2})/(\sigma_{V_{\text{Meas}}})$, number of standard deviation by which Bell's inequality is violated. Finally, the visibility V is V_{Meas} corrected for the limited visibility $w = 0.95$ of the interferometers: $V = V_{\text{Meas}}/w$.

Table 2. Comparison between Room Temperature, Integrated Entangled Photon Sources[a]

Reference	Structure	Material	Device Area (μm^2)	SNR	Spectral Brightness ($P = 1$ mW)
[11]	Waveguide	PPLN	~180000	~6[b]	~7.5×10^7 (s^{-1} nm^{-1})
[34]	Waveguide	AlGaAs	~10000	~7[c]	~6×10^5 (s^{-1} nm^{-1})
[15]	Waveguide	Si	~5000	~30	~4×10^5 (s^{-1} nm^{-1})
[16]	CROW	Si	~8000	~8	~3×10^6 (s^{-1} nm^{-1})
Present work	μ Ring	Si	~300	~64	~6×10^7 (s^{-1} nm^{-1})

[a]The values of spectral brightness refer to the coupled pump power and the internal generation rate.
[b]The SNR is inferred from the HOM experiment reported in the article.
[c]The SNR is calculated from the experimental value of the fidelity reported in the article.

A further advantage of the source reported here is that ring resonators are also a well-established industrial standard, already used in modulators. Here we have demonstrated a new, compelling functionality of ring resonators: they can be used as sources of entangled states of light. Immediate applications should follow, especially because their production readiness gives them advantages even over structures characterized by larger nonlinearities, but with less mature integration technologies [21]. The signal and idler beams have a bandwidth of ~13 GHz, which would allow their use in DWDM network systems without the need for any spectral filtering; the pump powers used here, on the order of dBm, are characteristic of those used in fiber networks; and the pump, signal, and idler frequencies lie in the telecommunications band. We can confidently expect that silicon mircoring resonators will become the dominant paradigm of correlated photon sources for quantum photonics, both for applications involving the transmission of quantum correlations over long distances, such as quantum cryptography, and for applications involving quantum information processing "on-a-chip."

FUNDING INFORMATION

Engineering and Physical Sciences Research Council (EPSRC); Fondazione Cariplo (2010-0523); MIUR (RBFR08XMVY); Natural Sciences and Engineering Research Council of Canada (NSERC).

ACKNOWLEDGMENT

We acknowledge the technical staff of the James Watt Nanofabrication Centre at Glasgow University. J. E. Sipe acknowledges support from the Natural Sciences and Engineering Research Council of Canada. M. J. Strain and M. Sorel acknowledge support from the EPSRC, UK.

See Supplement 1 for supporting content.

REFERENCES

1. M. A. Nielsen and I. L. Chuang, *Quantum Computation and Quantum Information* (Cambridge University, 2000).
2. A. K. Ekert, "Quantum cryptography based on Bell's theorem," Phys. Rev. Lett. **67**, 661–663 (1991).
3. M. Curty, M. Lewenstein, and N. Lütkenhaus, "Entanglement as a precondition for secure quantum key distribution," Phys. Rev. Lett. **92**, 217903 (2004).
4. R. Jozsa and N. Linden, "On the role of entanglement in quantum-computational speed-up," Proc. R. Soc. A **459**, 2011–2032 (2003).
5. C. H. Bennett and G. Brassard, "Quantum cryptography: public key distribution and coin tossing," in *Proceedings of the IEEE International Conference on Computers, Systems and Signal Processing* (IEEE, 1984), pp. 175–179.
6. A. Crespi, R. Ramponi, R. Osellame, L. Sansoni, I. Bongioanni, F. Sciarrino, G. Vallone, and P. Mataloni, "Integrated photonic quantum gates for polarization qubits," Nat. Commun. **2**, 566 (2011).
7. B. J. Metcalf, N. Thomas-Peter, J. B. Spring, D. Kundys, M. A. Broome, P. C. Humphreys, X. Jin, M. Barbieri, W. S. Kolthammer, J. C. Gates, B. J. Smith, N. K. Langford, P. G. R. Smith, and I. A. Walmsley, "Multiphoton quantum interference in a multiport integrated photonic device," Nat. Commun. **4**, 1356 (2013).
8. P. J. Shadbolt, M. R. Verde, A. Peruzzo, A. Politi, A. Laing, M. Lobino, J. C. F. Matthews, M. G. Thompson, and J. L. O'Brien, "Generating, manipulating and measuring entanglement and mixture with a reconfigurable photonic circuit," Nat. Photonics **6**, 45–49 (2011).
9. J. W. Silverstone, D. Bonneau, K. Ohira, N. Suzuki, H. Yoshida, N. Iizuka, M. Ezaki, C. M. Natarajan, M. G. Tanner, R. H. Hadfield, V. Zwiller, G. D. Marshall, J. G. Rarity, J. L. O'Brien, and M. G. Thompson, "On-chip quantum interference between silicon photon-pair sources," Nat. Photonics **8**, 104–108 (2013).
10. P. G. Kwiat, K. Mattle, H. Weinfurter, and A. Zeilinger, "New high-intensity source of polarization-entangled photon pairs," Phys. Rev. Lett. **75**, 4337–4341 (1995).
11. G. Fujii, N. Namekata, M. Motoya, S. Kurimura, and S. Inoue, "Bright narrowband source of photon pairs at optical telecommunication wavelengths using a type-II periodically poled lithium niobate waveguide," Opt. Express **15**, 12769–12776 (2007).
12. E. Pomarico, B. Sanguinetti, N. Gisin, R. Thew, H. Zbinden, G. Schreiber, A. Thomas, and W. Sohler, "Waveguide-based OPO source of entangled photon pairs," New J. Phys. **11**, 113042 (2009).
13. N. Matsuda, H. Le Jeannic, H. Fukuda, T. Tsuchizawa, W. J. Munro, K. Shimizu, K. Yamada, Y. Tokura, and H. Takesue, "A monolithically integrated polarization entangled photon pair source on a silicon chip," Sci. Rep. **2**, 817 (2012).
14. L. Olislager, J. Safioui, S. Clemmen, K. P. Huy, W. Bogaerts, R. Baets, P. Emplit, and S. Massar, "Silicon-on-insulator integrated source of polarization-entangled photons," Opt. Lett. **38**, 1960–1962 (2013).
15. K. Harada, H. Takesue, H. Fukuda, T. Tsuchizawa, T. Watanabe, K. Yamada, Y. Tokura, and S. Itabashi, "Generation of high-purity entangled photon pairs using silicon wire waveguide," Opt. Express **16**, 20368–20373 (2008).
16. H. Takesue, N. Matsuda, E. Kuramochi, and N. Masaya, "Entangled photons from on-chip slow light," Sci. Rep. **4**, 3913 (2014).
17. W. Tittel, J. Brendel, H. Zbinden, and N. Gisin, "Quantum cryptography using entangled photons in energy-time Bell states," Phys. Rev. Lett. **84**, 4737–4740 (2000).
18. I. Marcikic, H. de Riedmatten, W. Tittel, H. Zbinden, M. Legré, and N. Gisin, "Distribution of time-bin entangled qubits over 50 km of optical fiber," Phys. Rev. Lett. **93**, 180502 (2004).
19. J. Mower, Z. Zhang, P. Desjardins, C. Lee, J. H. Shapiro, and D. Englund, "High-dimensional quantum key distribution using dispersive optics," Phys. Rev. A **87**, 062322 (2013).

20. M. Davanço, J. R. Ong, A. B. Shehata, A. Tosi, I. Agha, S. Assefa, F. Xia, W. M. J. Green, S. Mookherjea, and K. Srinivasan, "Telecommunications-band heralded single photons from a silicon nanophotonic chip," Appl. Phys. Lett. **100**, 261104 (2012).
21. S. Azzini, D. Grassani, M. Galli, D. Gerace, M. Patrini, M. Liscidini, P. Velha, and D. Bajoni, "Stimulated and spontaneous four-wave mixing in silicon-on-insulator coupled photonic wire nano-cavities," Appl. Phys. Lett. **103**, 031117 (2013).
22. V. R. Almeida, C. A. Barrios, R. R. Panepucci, and M. Lipson, "All-optical control of light on a silicon chip," Nature **431**, 1081–1084 (2004).
23. S. Clemmen, K. Phan Huy, W. Bogaerts, R. G. Baets, P. Emplit, and S. Massar, "Continuous wave photon pair generation in silicon-on-insulator waveguides and ring resonators," Opt. Express **17**, 16558–16570 (2009).
24. J. E. Sharping, K. F. Lee, M. A. Foster, A. C. Turner, B. S. Schmidt, M. Lipson, A. L. Gaeta, and P. Kumar, "Generation of correlated photons in nanoscale silicon waveguides," Opt. Express **14**, 12388–12393 (2006).
25. C. Xiong, C. Monat, A. S. Clark, C. Grillet, G. D. Marshall, M. J. Steel, J. Li, L. O'Faolain, T. F. Krauss, J. G. Rarity, and B. J. Eggleton, "Slow-light enhanced correlated photon pair generation in a silicon photonic crystal waveguide," Opt. Lett. **36**, 3413–3415 (2011).
26. S. Azzini, D. Grassani, M. J. Strain, M. Sorel, L. G. Helt, J. E. Sipe, M. Liscidini, M. Galli, and D. Bajoni, "Ultra-low power generation of twin photons in a compact silicon ring resonator," Opt. Express **20**, 23100–23107 (2012).
27. E. Engin, D. Bonneau, C. M. Natarajan, A. S. Clark, M. G. Tanner, R. H. Hadfield, S. N. Dorenbos, V. Zwiller, K. Ohira, N. Suzuki, H. Yoshida, N. Iizuka, M. Ezaki, J. L. O'Brien, and M. G. Thompson, "Photon pair generation in a silicon micro-ring resonator with reverse bias enhancement," Opt. Express **21**, 27826–27834 (2013).
28. S. Azzini, D. Grassani, M. Galli, L. C. Andreani, M. Sorel, M. J. Strain, L. G. Helt, J. E. Sipe, M. Liscidini, and D. Bajoni, "From classical four-wave mixing to parametric fluorescence in silicon micro-ring resonators," Opt. Lett. **37**, 3807–3809 (2012).
29. I. Marcikic, H. de Riedmatten, W. Tittel, V. Scarani, H. Zbinden, and N. Gisin, "Time-bin entangled qubits for quantum communication created by femtosecond pulses," Phys. Rev. A **66**, 062308 (2002).
30. J. D. Franson, "Bell inequality for position and time," Phys. Rev. Lett. **62**, 2205–2208 (1989).
31. J. D. Franson, "Two photon interferometry over large distances," Phys. Rev. A **44**, 4552–4555 (1991).
32. D. Grassani, M. Galli, and D. Bajoni, "Active stabilization of a Michelson interferometer at an arbitrary phase with subnanometer resolution," Opt. Lett. **39**, 2530–2533 (2014).
33. P. G. Kwiat, A. M. Steinberg, and R. Y. Chiao, "High-visibility interference in a Bell-inequality experiment for energy and time," Phys. Rev. A **47**, R2472–R2475 (1993).
34. A. Orieux, A. Eckstein, A. Lemaître, P. Filloux, I. Favero, G. Leo, T. Coudreau, A. Keller, P. Milman, and S. Ducci, "Direct Bell states generation on a III–V semiconductor chip at room temperature," Phys. Rev. Lett. **110**, 160502 (2013).
35. N. C. Harris, D. Grassani, A. Simbula, M. Pant, M. Galli, T. Baehr-Jones, M. Hochberg, D. Englund, D. Bajoni, and C. Galland, "An integrated source of spectrally filtered correlated photons for large scale quantum photonic systems," arXiv:1409.8215v1, 2014.